machines

MDPI

Article

Design and Experimental Study on the Torque Balancing Mechanism of a Satellite-Borne Two-Axis Rotary Table

Yuzhe Wang [1,2], Xiaodong Sui [1,2], Tianqing Zhang [1,2], Ting Nie [1] and Changzheng Chen [1,*]

[1] Changchun Institute of Optics, Fine Mechanics and Physics, Chinese Academy of Sciences, Changchun 130033, China; wangyuzhe19@mails.ucas.ac.cn (Y.W.); suixiaodong21@mails.ucas.ac.cn (X.S.); zhangtianqing18@mails.ucas.ac.cn (T.Z.); nieting@ciomp.cn (T.N.)
[2] University of Chinese Academy of Sciences, Beijing 100049, China
* Correspondence: chencz@ciomp.ac.cn

Abstract: With the rapid development of science and technology, high-resolution remote sensing cameras are now widely used in various fields. At the beginning of camera attitude adjustment, residual torque due to state changes can affect platform stability and lead to the degradation of imaging quality. This paper analyzes the effect of external disturbances on the attitude of the satellite platform according to the Newton–Euler method. In order to effectively realize the self-balancing of the torque of the remote sensing camera rotary table and eliminate the influence of the residual torque on the stability of the satellite platform, this study designs a torque balancing mechanism for the two-axis rotary table of a remote sensing camera based on the first-generation balancing mechanism. Firstly, this paper provides a detailed analysis of the mechanism equilibrium principle from the theoretical point of view based on the theories related to momentum moment theorem and momentum moment conservation law. Then, the dynamics model of the torque balancing mechanism is built, and the dynamics simulation analysis is carried out in this paper. The analysis results show that compared with the first-generation torque balancing mechanism, the residual torque of the second-generation torque balancing mechanism is reduced by 66.67%, the peak value of the residual torque is reduced by 57.55%, the mass of the balancing flywheel is reduced by 74.14%, and the torque balancing time is reduced by 42.86%. Finally, two torque balancing mechanism prototypes were fabricated at equal scale for test verification in this paper. The test results show that compared with the first-generation torque balancing mechanism, the residual torque of the second-generation test prototype is reduced by 40%, the peak of the residual torque is reduced by 25%, the mass of the balancing flywheel is reduced by 60.34%, and the torque balancing time is reduced by 51.06%. There are some differences between the simulation analysis and the experimental results, but the overall trend is consistent with the theory. Through theoretical derivation, simulation analysis and experimental verification, the correctness and feasibility of the proposed second-generation torque balancing mechanism are fully confirmed, which has certain reference significance and engineering application value for the torque self-balancing scheme of rotary tables.

Keywords: satellite attitude; Newton–Euler method; conservation of momentum; torque analysis; balancing mechanism

Citation: Wang, Y.; Sui, X.; Zhang, T.; Nie, T.; Chen, C. Design and Experimental Study on the Torque Balancing Mechanism of a Satellite-Borne Two-Axis Rotary Table. *Machines* **2023**, *11*, 830. https://doi.org/10.3390/machines11080830

Academic Editor: Dan Zhang

Received: 30 June 2023
Revised: 2 August 2023
Accepted: 9 August 2023
Published: 15 August 2023

1. Introduction

With the rapid development of space technology, remote sensing cameras are playing an increasingly important role in resource census, environmental monitoring, terrain mapping, astronomical observation, target tracking, and other fields while also developing in the direction of miniaturization and light weight [1–4]. Due to the weightless environmental conditions in space, especially for some high-resolution remote sensing cameras, the key to ensuring the performance of the camera lies in how to avoid the influence of the active load motion on the satellite attitude and maintain the stability of the satellite

platform as well as the pointing accuracy. The problem of satellite interference by onboard active payloads has been a long-standing concern for researchers [5–7]. Dae-Kwan Kim [8] introduced a micro-vibration model for reaction wheel assembly by analyzing the coupled flywheel model and the empirical interference model and successfully applied them to a commercial reaction wheel assembly, while he also proposed a procedure for the parameter estimation of coupled models from micro-vibration perturbation data. Li Kang and Zhang Honghua [9] proposed a subspace-based system identification method for flexible spacecraft to extract both unperturbed dynamics and unknown periodic perturbation patterns; the proposed method can be extended to identify systems containing uncontrollable but observable states and to separate these uncontrollable states from other states. J.A.A. Engelbrecht [10] presented two methods for the on-orbit identification of unmodelled disturbing torques acting on a spacecraft body, through which the identified disturbing torques can be analyzed and modelled to improve the attitude dynamics model of the spacecraft. Neil E. Goodzeit [11] proposed a method that can determine the control-output dynamics of a flexible spacecraft when subjected to single or multiple periodic interferences; the method uniquely separates the effects of control excitation from the effects of unknown periodic perturbations in order to correctly identify control-output dynamics and perturbation effects. The above study mainly investigated the interference identification and estimation of the active load on the satellite platform and did not analyze the effect of the interference on the attitude of the satellite platform. In this paper, the attitude dynamics of a satellite platform with a rotating body device is analyzed based on the Newton–Euler method while neglecting the external moments of the space environment during the operation of the satellite.

In current space remote sensing applications, remote sensing cameras are rigidly connected to the satellite platform. To achieve imaging of the target point of interest, it is often necessary in engineering to adjust the attitude of the entire satellite by means of a reaction flywheel or torque gyroscope in the satellite platform [12–14]. This imaging method not only requires a platform with high maneuverability, but also increases wear and tear on the flywheel and gyroscope, and there are micro-vibration disturbances in the flywheel, which rotates at high speed for a long time [15–19]. In order to reduce the wear and tear of the flywheel, realize the simultaneous imaging of multiple cameras and targets, and improve the rapid response capability of the cameras, this paper adopts the remote sensing camera rotary table to adjust the attitude of the cameras in orbit. In the area of rotary table research, Lihua Wang [20] designed a neural network PID control system based on the operating environment characteristics of a space laser communication tracking rotary table. The control system can self-adjust the parameters under the change of the mathematical model of the object, solving the problem of controlling the change of the object model in space. It also solves the problem of accuracy degradation caused by vibration and disturbances by finding the best control method through the self-learning function of neural networks. Gan Ke-li [21] used two compensating wheels to offset the spatial flywheel momentum under the condition that the inertia characteristics of the rotating part are changed. Qin Tao [22] conducted a structural optimization design and stiffness analysis of a satellite-borne two-axis rotary table, and the mechanical properties of the design solution meet the task requirements of laser communication. Scholars have studied more on the optimal design of satellite-borne rotary table structure and control systems and less on how to reduce or eliminate the disturbing torque introduced during the operation of the rotary table.

Remote sensing cameras have high requirements for platform stability. Any small shake will affect the image quality of the camera. Remote sensing cameras are external payloads compared with satellite platforms. When the camera is in the process of adjustment, the change of the camera motion state will introduce additional disturbances, which have a certain impact on the stability of the platform, and the image quality of the camera is reduced. In order to solve the above problems, this paper designs and analyzes the second-generation torque balancing mechanism based on the first-generation torque

balancing mechanism. The mechanism frees up the stator's degrees of freedom and uses the rotor and stator to drive the balanced flywheel and load rotation, respectively. There are significant improvements in residual torque balancing time, balancing effect, and light weight, which effectively guarantee the stability of the satellite platform.

The paper consists of seven sections. Section 2 analyzes the effect of external loads on the satellite platform; Section 3 introduces the working principle of the torque balancing mechanism and provides a theoretical analysis; Section 4 analyzes the dynamics of the torque balancing mechanism; Section 5 describes the test work on the torque balancing mechanism; Section 6 discusses sources of experimental error and directions for future research; and Section 7 summarizes the overall work of this paper.

2. Effect of External Torque on Satellite Attitude

A remote sensing camera is a comprehensive instrument with optical, mechanical, electronic, temperature, and other technologies, which is widely used in various fields. A two-axis rotary table is a pointing adjustment mechanism, adjusting the camera pointing through the rotation of the pitch and azimuth axis to complete the imaging task. It has the advantages of independent adjustment of camera pointing, not interfering with the normal work of other instruments, reducing the mass of the whole star, as shown in Figure 1. In the weightless conditions of space, any small interference will have a huge impact on the stability of the satellite platform. The remote sensing camera is an external component relative to the platform, the unbalanced torque during the rotation of the rotary table can be considered as an applied disturbance, and the derivation of the kinematic and dynamical equations of the satellite attitude helps to study the effect of external torque on the attitude of the satellite.

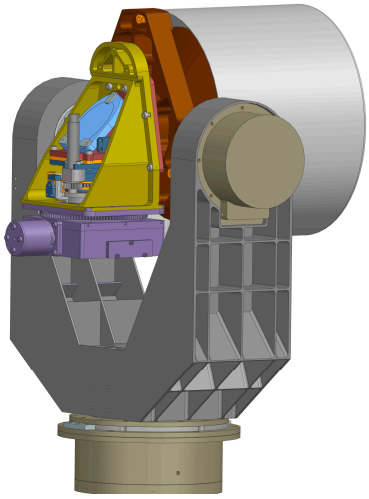

Figure 1. Schematic diagram of the entire camera system.

2.1. Definition of the Reference Coordinate System

Defining the space reference coordinate system can determine the satellite's position, velocity, angle, and other relevant information in space; therefore, multiple coordinate systems should be established to accurately describe the attitude of a satellite platform when studying its attitude. In this paper, the following coordinate systems are defined.

1. Geocentric inertial coordinate system $O_iX_iY_iZ_i$

Take the geocentric inertial coordinate system as the geocenter O_i, the O_iX_i-axis is centered in the equatorial plane pointing towards the equinox, O_iZ_i-axis is the earth's rotation axis, and the O_iY_i-axis is determined by the O_iX_i-axis and the O_iZ_i-axis through the right-handed spiral rule. This coordinate system is used to describe the state of the satellite in inertial space, as shown in Figure 2.

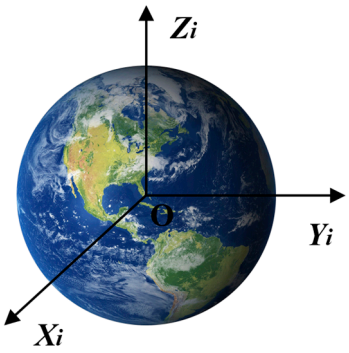

Figure 2. Schematic diagram of the geocentric inertial coordinate system.

2. Orbital coordinate system $OX_oY_oZ_o$

The orbital coordinate system is a coordinate system determined by the orbital plane, with the origin O at the center of mass of the satellite, the OZ_o-axis points to the center of the earth, the OX_o-axis is perpendicular to the OZ_o-axis in the orbital plane and points in the direction of the satellite's velocity, and the OY_o-axis is determined by the other two axes through the right-handed spiral rule. This coordinate system is used to describe the satellite orbit state, as shown in Figure 3.

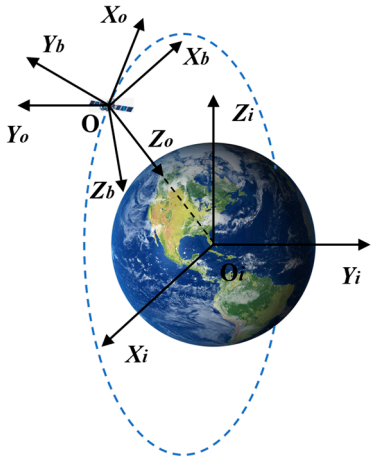

Figure 3. Schematic diagram of the orbital coordinate system and the satellite body coordinate system.

3. Satellite body coordinate system $OX_bY_bZ_b$

The satellite body coordinate system is fixed on the satellite body, with the origin O at the center of mass of the satellite, and the three axes are aligned with the main axis of inertia of the satellite. For Earth-directed satellites, the system coincides with the orbital system when the satellite has no attitude deviation, te OX_b-axis points in the direction of the satellite's flight and is called the roll axis, the OZ_b-axis points in the direction of the center of the Earth and is called the yaw axis, and OY_b-axis and the other two axes form a right-handed right-angle coordinate system, called the pitch axis, as shown in Figure 3.

2.2. Attitude Description and Kinematic Equations of Satellites Based on Euler Angles

The description of Euler's angle is derived from Euler's theorem; this means that the angular displacement of a rigid body around a fixed point can be synthesized from a number of finite rotations around that point, and it is characterized by its intuitiveness and the minimal implementation of the attitude description. Therefore, the satellite body coordinate system can be obtained by rotating the reference system around different coordinate axes three times in succession, the axis of rotation for each time is taken to be one of the axes of the rotated coordinate system, and the angle of rotation for each time is called the Euler angle.

Use the orbital coordinate system as the reference coordinate system and use the $Z-X-Z$ rotation method to convert the coordinate system; the angle of each rotation is ψ, θ, φ, as shown in Figure 4.

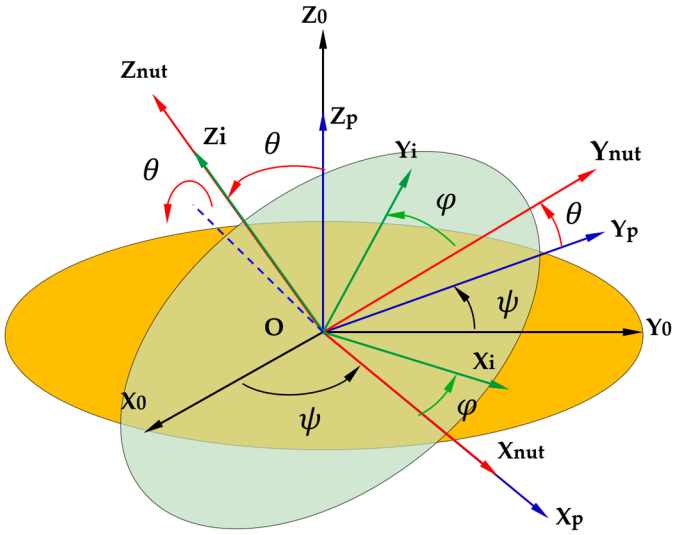

Figure 4. Schematic diagram of coordinate system transformation.

The transformation matrix of the three rotations is obtained from the transformation relation as:

$$M_{op}(\psi) = \begin{bmatrix} \cos\psi & -\sin\psi & 0 \\ \sin\psi & \cos\psi & 0 \\ 0 & 0 & 1 \end{bmatrix} \tag{1}$$

$$M_{p,nut}(\theta) = \begin{bmatrix} 1 & 0 & 0 \\ 0 & \cos\theta & -\sin\theta \\ 0 & \sin\theta & \cos\theta \end{bmatrix} \tag{2}$$

$$M_{nut,i}(\varphi) = \begin{bmatrix} \cos\varphi & -\sin\varphi & 0 \\ \sin\varphi & \cos\varphi & 0 \\ 0 & 0 & 1 \end{bmatrix} \tag{3}$$

Then, the transformation matrix obtained from the $Z-X-Z$ order is derived as:

$$\begin{aligned} M_{oi}(\psi,\theta,\varphi) &= M_{op}(\psi)M_{p,nut}(\theta)M_{nut,i}(\varphi) \\ &= \begin{bmatrix} \cos\psi\cos\varphi - \sin\psi\cos\theta\sin\varphi & -\cos\psi\sin\varphi - \sin\psi\cos\theta\cos\varphi & \sin\psi\sin\theta \\ \sin\psi\cos\varphi + \cos\psi\cos\theta\sin\varphi & -\sin\psi\sin\varphi + \cos\psi\cos\theta\cos\varphi & -\cos\psi\sin\theta \\ \sin\theta\sin\varphi & \sin\theta\cos\varphi & \cos\theta \end{bmatrix} \end{aligned} \tag{4}$$

Let ω denote the angular velocity of rotation of the satellite body coordinate system relative to the geocentric inertial coordinate system; ω_{ob} denotes the angular velocity of rotation of the satellite body coordinate system relative to the orbital coordinate system. They are represented in the orbital coordinate system as:

$$\omega = \left[\omega_x, \omega_y, \omega_z\right]^T, \quad \omega_{ob} = \left[\omega_{obx}, \omega_{oby}, \omega_{obz}\right]^T \tag{5}$$

ω_i is the angular velocity of rotation of the orbital coordinate system with respect to the geocentric inertial coordinate system and is expressed in the orbital coordinate system as:

$$\omega_i = [0, -\omega_o, 0]^T \tag{6}$$

where ω_0 is the orbital angular velocity. Therefore, the kinematic equation of the satellite attitude based on the Euler angle can be derived as:

$$\omega = \omega_{ob} + M_{oi}(\psi, \theta, \varphi)\omega_i \tag{7}$$

So:

$$\begin{bmatrix} \omega_x \\ \omega_y \\ \omega_z \end{bmatrix} = \begin{bmatrix} \dot{\theta}\cos\psi + \dot{\varphi}\sin\psi\sin\theta + \omega_0(\cos\psi\sin\varphi + \sin\psi\cos\theta\cos\varphi) \\ \dot{\theta}\sin\psi - \dot{\varphi}\cos\psi\sin\theta - \omega_0(\cos\psi\cos\theta\cos\varphi - \sin\psi\sin\varphi) \\ \dot{\psi} + \dot{\varphi} - \omega_0\sin\theta\cos\varphi \end{bmatrix} \tag{8}$$

2.3. Perturbation Analysis of Satellite Attitude by External Torque

Assume that the satellite is a rigid body, then the dynamic equations of the satellite attitude can be derived by the Newton–Euler method. Let H_Σ be the torque of the whole satellite with respect to its own center of mass and T_Σ be the combined moment of the external forces with respect to the center of mass of the satellite; then, according to the Newton–Euler method:

$$\frac{dH_\Sigma}{dt} = T_\Sigma \tag{9}$$

Using the satellite body coordinate system as the computational coordinate system, from the vector relative derivative equation, there is:

$$\dot{H_\Sigma} + \omega \times H_\Sigma = T_\Sigma \tag{10}$$

where H_Σ is the torque of the whole star and T_Σ is the total torque applied to the star, expressed as following:

$$T_\Sigma = T_c + T_n \tag{11}$$

where T_c is the control torque applied to the star and T_n is the various external interference torques to the satellite.

The star rotational inertia array is I, so $H = I\omega$ and the dynamics equation of the satellite platform attitude can be expressed as:

$$I\dot{\omega} + \omega \times (I\omega) = T_c + T_n \tag{12}$$

The satellite body coordinate system is consistent with the satellite inertial principal axis, and I can be considered as a diagonal matrix, recorded as $I = diag(I_x\ I_y\ I_z)$, T_c and T_n are noted as:

$$\begin{cases} T_c = \begin{bmatrix} T_{cx}\ T_{cy}\ T_{cz} \end{bmatrix}^T \\ T_n = \begin{bmatrix} T_{nx}\ T_{ny}\ T_{nz} \end{bmatrix}^T \end{cases} \tag{13}$$

Then, Equation (12) can be expanded as:

$$\begin{cases} I_x\dot{\omega_x} - (I_y - I_z)\omega_y\omega_z = T_{cx} + T_{nx} \\ I_y\dot{\omega_y} - (I_z - I_x)\omega_z\omega_x = T_{cy} + T_{ny} \\ I_z\dot{\omega_z} - (I_x - I_y)\omega_x\omega_y = T_{cz} + T_{nz} \end{cases} \tag{14}$$

In this paper, the external torques such as the gravitational gradient torque and aerodynamic torque of the satellite in orbit are ignored, so $T_n = \begin{bmatrix} T_{nx}\ T_{ny}\ T_{nz} \end{bmatrix}^T = [0\ 0\ 0]^T$ and Equation (14) can be simplified as:

$$\begin{cases} I_x\dot{\omega_x} - (I_y - I_z)\omega_y\omega_z = T_{cx} \\ I_y\dot{\omega_y} - (I_z - I_x)\omega_z\omega_x = T_{cy} \\ I_z\dot{\omega_z} - (I_x - I_y)\omega_x\omega_y = T_{cz} \end{cases} \tag{15}$$

3. Research on the Torque Balancing Mechanism of Two-Axis Rotary Tables

As a carrier for remote sensing cameras, a satellite platform usually carries multiple remote sensing cameras; disturbing moments caused by the drive torque when the camera is adjusted to its working attitude by means of a rotary table can lead to image quality degradation. To address the above situation, this paper proposes a torque balancing mechanism of a two-axis rotary table; this mechanism eliminates the effect of disturbing moments on the stability of the satellite platform. The relationship between the three axes of the rotary table is shown in Figure 5.

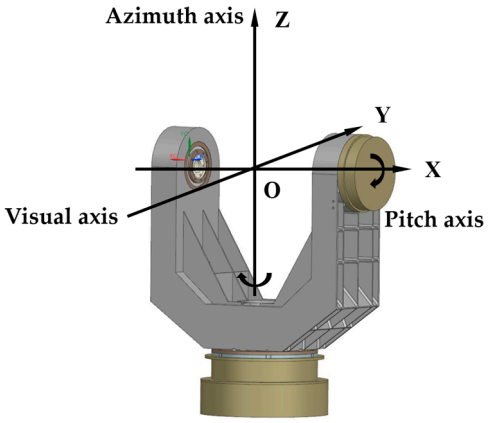

Figure 5. Three axes' rotation relationship of the rotary table.

3.1. Structure Design of the Torque Balancing Mechanism of the Rotary Table

As an important structure for adjusting the attitude of a remote sensing camera, the main components of the rotary table are the drive motor, transmission structure, transmission, and so on. Torque is often generated in the process of the motor starting, so the balance flywheel can be used to eliminate the torque. Torque balancing mechanisms are generally available in two options: (1) the motor drives the balancing wheel and the rotary table respectively, thus realizing torque self-balancing. However, this balancing method usually has a complex structure and greatly increases the weight and control difficulty of the whole machine, which raises the manufacturing and research costs; (2) use the motor's rotor to drive the transmission while driving the rotating shaft and torque balancing wheel to achieve the balancing effect; this method has been verified and applied in engineering at present. Based on this balanced scheme, the second-generation torque balancing mechanism for the rotary table of a remote sensing camera proposed in this paper mainly consists of the following components: a brushless motor, rotating spindle, housing, planetary wheel system, and torque balance wheel. We used a planetary wheel system instead of a speed increaser to change the speed increment ratio according to the actual engineering needs. The structure of the second-generation torque balancing mechanism for the rotary table of a remote sensing camera is shown in Figure 6.

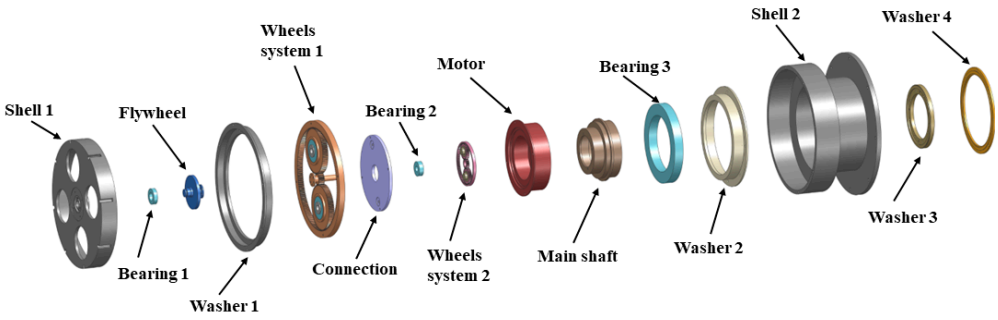

Figure 6. Structure diagram of the second-generation torque balancing mechanism.

The working principle of the second-generation rotary table torque balancing mechanism is explained as follows: components of the remote sensing camera rotary table torque balancing mechanism are fixed in the housing, and the housing is connected to the satellite body through the connector, and a brushless motor is used as the power input. Unlike the first-generation mechanism in which the motor stator remained fixed, this mechanism releases the axially rotational degree of freedom of the motor stator; using the mutual reaction electromagnetic torque between the rotor and stator in the energized state of the motor, the stator drives the spindle rotation, and the rotor realizes the torque balance flywheel rotation commutation and acceleration rotation through the planetary wheel system. In this balancing mechanism, the stator and rotor are used as "power sources" to drive the spindle and flywheel to complete the attitude adjustment of the remote sensing camera and the torque balancing of the rotary table, respectively. Due to the release of the axially rotational degree of freedom of the drive motor stator, the contact between internal and external components is reduced, which reduces the output of residual torque and achieves torque balance more effectively on the premise of ensuring the completion of the task.

3.2. Theoretical Analysis of Rotary Table Torque Balancing Mechanism

In order to verify the theoretical feasibility of the torque balancing mechanism proposed in this paper, the relevant theoretical analysis is carried out according to the momentum moment theorem and the law of conservation of momentum moment. With the motor energized, the rotor of the motor applies a counterclockwise torque M_t to the wheelset assembly. At the same time, the stator of the motor applies a clockwise torque M_t' to the spindle, driving the spindle counterclockwise. Here, this paper takes the main components of the balancing mechanism as the object of study for force analysis, and the force analysis is shown in Figure 7.

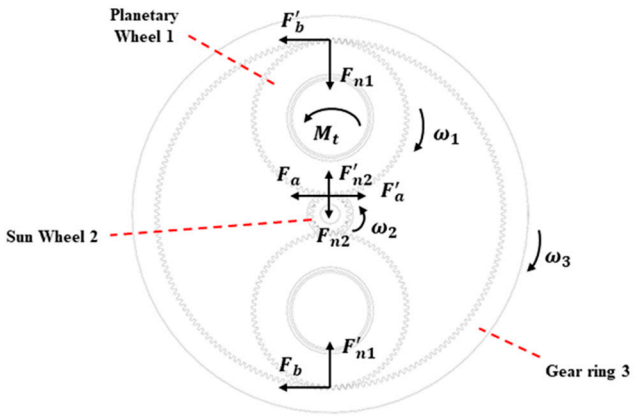

Figure 7. Diagram of force analysis.

Due to the release of the motor stator, the contact connection between the drive mechanism and the outside is optimized in the structure, and the output point of the internal structure to the shell is only the contact point between the gear ring and the shell, which reduces the output of external torque, and the whole mechanism is better balanced. In this paper, planetary wheel 1 is subjected to a counterclockwise force F_a', counterclockwise force F_b', and counterclockwise moment M_t, solar wheel 2 is subjected to a counterclockwise force F_a, the clockwise force on gear ring 3 is denoted as F_b, and the

residual torque of the torque balancing mechanism of the remote sensing camera rotary table is recorded as $M(t)$, so:

$$\begin{cases} F_a' \cdot r_2 - F_b'(2r_1 + r_2) = M_t - J_1 \frac{d\omega_1(t)}{dt} \\ \left(J_2 + J_f\right) \frac{d\omega_2(t)}{dt} = 2F_a \cdot r_2 \\ J_m \frac{d\omega_m(t)}{dt} = M_d \\ M_t + J_p \frac{d\omega_p(t)}{dt} = M_d \\ M(t) = F_b \cdot (2r_1 + r_2) \end{cases} \tag{16}$$

Solving the above equation yields:

$$M(t) = \frac{J_2 + J_f}{2} \cdot \frac{d\omega_2(t)}{dt} + J_p \frac{d\omega_p(t)}{dt} + J_1 \frac{d\omega_1(t)}{dt} - J_m \frac{d\omega_m(t)}{dt} \tag{17}$$

where J_m is the spindle inertia, ω_m is the spindle angular velocity, J_1 is the inertia of the planetary wheel, ω_1 is the angular velocity of the planetary wheel, r_1 is the radius of the planetary wheel, J_2 is the rotational moment of inertia of the sun wheel, ω_2 is the rotational angular velocity of the sun wheel, r_2 is the radius of the sun wheel, J_p is the rotor joint rotational inertia, ω_p is the rotor joint rotational angular velocity, and J_f is the balance wheel rotational inertia.

Equation (17) shows that the residual torque $M(t)$ of the torque balancing mechanism is related to the properties of each component itself and the angular acceleration. In order to balance the torque of the rotary table mechanism, i.e., to achieve zero residual torque on the satellite platform, we can change the rotational inertia of the rotating parts or the size of the wheel system or adjust the angular acceleration of the relevant rotating parts. From the above analysis, based on the theory related to momentum moment theorem and momentum moment conservation law, it is proven that the torque balancing mechanism proposed in this paper is correct in principle and feasible in design.

4. Simulation Analysis of the Two-Axis Rotary Table Torque Balancing Mechanism

4.1. Mathematical Model of the Balancing Mechanism Motor

A brushless motor is selected as the driving mechanism for the torque balancing mechanism of the remote sensing camera rotary table. In order to simplify the process of analysis, the following assumptions are made in this paper in the process of establishing the mathematical model of the motor drive system: ignore the tooth slot effect of the brushless motor and motor core saturation; ignore the eddy current and hysteresis loss of the brushless motor; energy is conserved throughout the process; and ignore the influence of friction in the transmission process. Then, the mathematical model of the motor is:

$$\begin{cases} u(t) = 2Ri(t) + 2L\frac{di(t)}{dt} + e_o \\ e_o = 2E \\ M_d = \frac{2k_e n}{\omega_m} i = k_t i \\ M_d - T_L = J\frac{d\omega_m(t)}{dt} + B\omega_m(t) \end{cases} \tag{18}$$

where $u(t)$ is the equivalent input voltage of the motor, R is the motor winding equivalent resistance, L is the motor winding equivalent inductance, $i(t)$ is the motor equivalent input current, e_o is the ideal counter-electromotive force, E is the counter-electromotive force amplitude, M_d is the electromagnetic torque, k_e is the counter-electromotive force coefficient, ω_m is the mechanical angular velocity of the rotor, J is the equivalent rotational inertia of the motor, T_L is the friction torque generated by external friction, and B is the coefficient of viscous friction.

In this study, the frictional effect in the transmission process is neglected, and the electromagnetic torque M_d is considered as the input torque of the whole mechanical structure, and its value is determined by the overall rotational inertia and angular acceleration of

the camera. Since the stator has the freedom to rotate around the central axis, this paper considers that the torques applied to the rotor and stator in the energized case are each other's reaction torques, which are equal in magnitude and opposite in direction.

4.2. Simulation Analysis of the Dynamics of the Rotary Table Torque Balancing Mechanism

In order to verify the feasibility of the torque balancing mechanism proposed in this paper and the correctness of the theoretical analysis, the dynamics of the torque balancing mechanism are simulated. In this paper, theoretical calculations are performed to derive the reasonable rotational inertia of each component so that the residual torque is zero and the internal torque of the structure is self-balanced. The rotational inertia of the main components of the balancing mechanism is shown in Table 1. As can be seen from Table 1, the rotational inertia of the components in the second-generation mechanism is significantly reduced compared to the first-generation mechanism. This is due to the fact that the release of the degrees of freedom of the motor's stator causes the camera and the balancing parts to turn differently, indirectly reducing the number of components that need to be balanced.

Table 1. Rotational inertia of the main components.

Part Name	Rotational Inertia kg·m^2	
	First-Generation Balancing Mechanism	Second-Generation Balancing Mechanism
Main Shaft	1.464×10^{-3}	1.071×10^{-3}
Planetary Wheel	1.472×10^{-3}	1.025×10^{-3}
Solar Wheel	2.268×10^{-3}	2.020×10^{-6}
Wheel System Connectors	5.186×10^{-3}	4.366×10^{-4}
Flywheel	1.293×10^{-3}	5.091×10^{-5}

This study uses UG-ADAMS joint simulation to analyze the dynamics of two balancing mechanisms and simplifies some of the parts. The planetary wheel system is generated by the detailed method, and realistic gearing is simulated based on the contact of geometric models. The constraints of the important parts in the two models are listed in Table 2, and the simulation model of the whole machine is shown in Figure 8.

Table 2. Constraints of important parts.

Constraint Name	Binding Type	Constraint Part 1	Constraint Part 2
Joint Shaft Load	Fixed	Shaft load	Connecting transition
Joint Flywheel	Revolute	Flywheel	Shell
Planet ring fixed	Fixed	Planet ring	Connecting transition
Planet 1 revolute	Revolute	Planet carrier	Planet planet gear 1
Planet ring planet force	General force	Planet ring	Planet planet gear 1/2
Planet carrier fixed	Fixed	Planet carrier	Rotor connecting
Planet ring fixed	Fixed	Planet ring	Shell
Joint Shaft Load	Revolute	Shaft load	Shell

4.3. Analysis of Dynamics Simulation Results

The observation point of torque output was selected at the center of the bottom of the balancing mechanism shell, and the output results of each observation of the dynamics analysis are shown in Figure 9, and the results of each observation are summarized in Table 3.

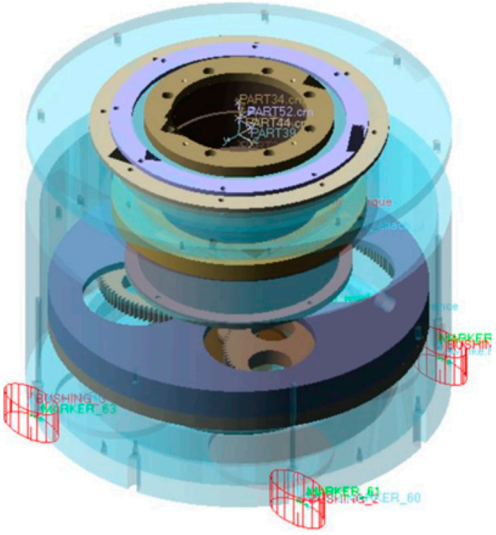

Figure 8. Simulation model of the whole machine dynamics.

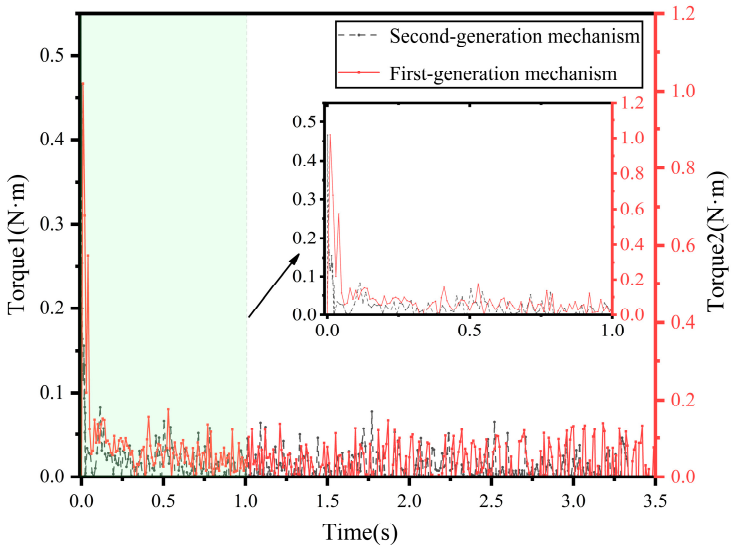

Figure 9. Output results of the simulation analysis.

Table 3. Comparison of the balancing mechanism output results.

Project Name	First-Generation Torque Balancing Mechanism	Second-Generation Torque Balancing Mechanism	Optimization Percentage (%)
Residual torque (N·m)	0.06	0.02	66.67
Peak of residual torque (N·m)	1.06	0.45	57.55
Mass of flywheel (kg)	0.58	0.15	74.14
Balancing time(s)	0.35	0.20	42.86

As can be seen in Figure 9, compared to the first-generation mechanism, the residual torque of the second-generation torque balancing mechanism proposed in this paper is 0.02 N·m, which is reduced by 66.67%, the peak of residual torque is 0.45 N·m, which is reduced by 57.55%, the mass of the balanced flywheel is 0.15 kg, which is reduced by 74.14%, and the moment balance time is 0.2 s, which is reduced by 42.86%. Through the above analysis, it can be seen that the torque balancing mechanism proposed in this paper has smaller residual torque, less influence on the stability of the satellite platform, shorter balancing and stabilization time, and a more sensitive response to the balancing effect

and can play a balancing effect faster. At the same time, the second-generation balancing mechanism can achieve torque balancing through the smaller size and mass of the balancing flywheel, which reduces the overall mass of the remote sensing camera and is conducive to the lightweight of the remote sensing camera, and it is of great significance in engineering applications. In summary, the feasibility and correctness of the torque balancing mechanism proposed in this paper are verified in terms of simulation analysis.

5. Test Verification of the Two-Axis Rotary Table Torque Balancing Mechanism

5.1. Wheel System Design of the Rotary Table Torque Balancing Mechanism

According to Equation (17), in order to enable the torque balancing mechanism to achieve a self-balancing state with zero residual torque under ideal conditions, the rotational inertia of each component and the incremental speed ratio of the planetary wheel system are first determined. Releasing the degree of freedom of rotation of the stator around the main shaft allows it to drive the spindle to rotate and realize the attitude adjustment of the remote sensing camera. The rotor's torque is input through the rotating shaft of the planetary wheel, and due to the speed-increasing characteristic of the turnover wheel system, the sun wheel is sped up, and then the sun wheel accelerates the rotation of the balance wheel to realize the self-balancing effect of the whole mechanism.

As the main component of the second-generation torque balancing mechanism proposed in this paper, the rotating wheel system needs to be designed in detail. In order to ensure the light weight and miniaturization of the whole mechanism, the number of teeth of the sun wheel is chosen to be as small as possible.

$$Z_{min} = \frac{2h_a^*}{\sin^2 \alpha} \tag{19}$$

From Equation (19), when $h_a^* = 1$, $\alpha = 20^\circ$, the minimum number of teeth can be 17 in order to avoid the heel cut phenomenon when machining the sun wheel. Due to the determination of the speed increase ratio, the parameters related to the planetary wheel and gear ring can be deduced separately, which are shown in Table 4.

Table 4. Parameters related to the planetary wheel system.

Part Name	Material	Number of Teeth	Tooth Top Height Factor	Pressure Angle (°)	Modulus
Solar wheel	Steel	20	1	20	1
Gear ring	Steel	180	1	20	1
Planetary wheel	Steel	80	1	20	1

5.2. Analysis of Test Results

After the basic parameters of the planetary wheel system are determined, according to the actual engineering needs, the motor is selected as a brushless motor with a maximum residual torque of 6 N·m, a rated voltage of 24 V, and a rated current of 4 A. In order to ensure the mounting accuracy, the bearings choose crossed roller bearings and deep groove ball bearings to better ensure the assembly accuracy and co-axiality of each component. In order to accurately and reasonably measure the residual torque of the balancing mechanism, a sensor is installed at the center of the bottom of the balancing mechanism housing to effectively measure each observation with the tooling, and the torque balance test is shown in Figure 10.

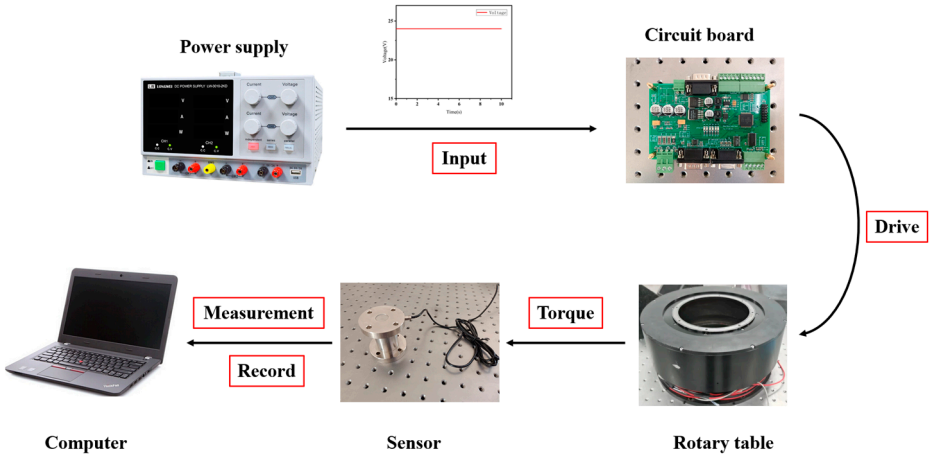

Figure 10. Test of torque balance.

In order to analyze the balancing effect of the second-generation torque balancing mechanism proposed in this paper, two kinds of torque balancing mechanisms are compared and tested. As can be seen from Equation (17), after the rotational inertia of each component is determined, a balance wheel with appropriate rotational inertia is reasonably designed for balancing according to the residual torque. In this test, the balancing mechanism is placed on the tooling table, which has axial degrees of freedom of rotation and can support the free rotation of the balancing mechanism. The torque sensor is installed at the bottom of the mechanism shell, the upper part of which can rotate freely with the mechanism and the lower part is fixed on the tooling to keep it stationary, which can measure the residual torque of the balancing mechanism in real time with an accuracy of 0.01 N·m and observe the torque balance through the residual torque curve. There are machining errors, assembly errors, and introduction errors in the process of the test; the above errors are accumulated and recorded as a combined error with a value of 8%. The test results are shown in Figure 11, and Table 5 compares the test results of the two torque balancing mechanisms.

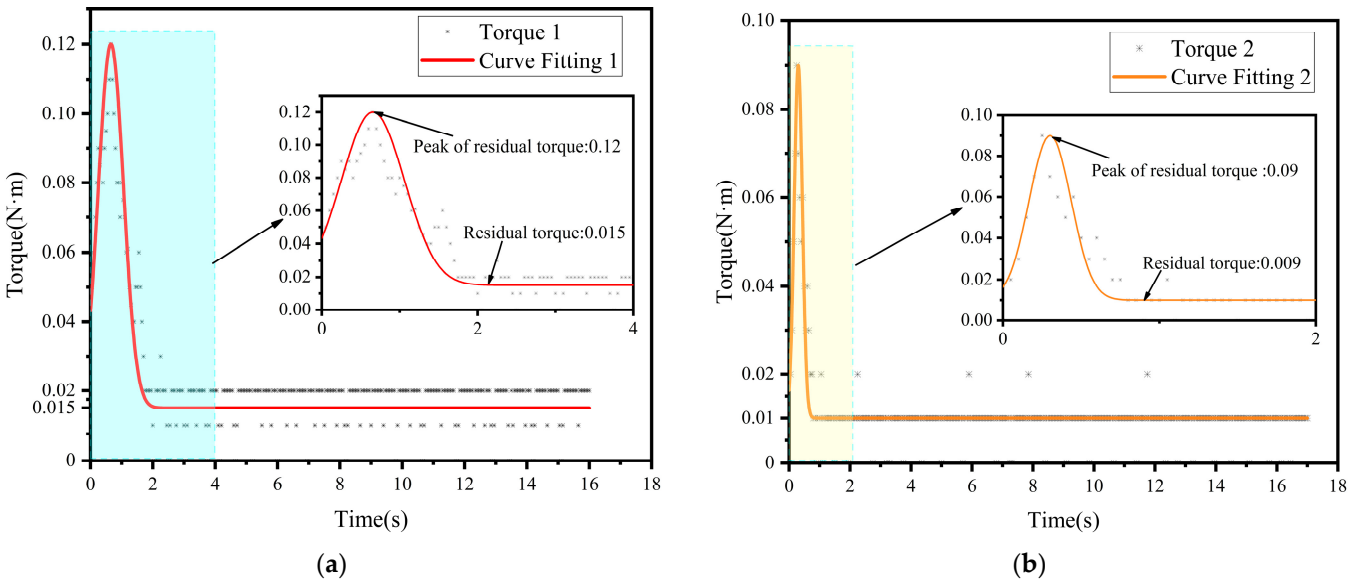

Figure 11. Results of the test: (**a**) the first-generation mechanism and (**b**) the second-generation mechanism.

Table 5. Comparison of test results of the balancing mechanisms.

Institution Name / Test Items	First-Generation Torque Balancing Mechanism	Second-Generation Torque Balancing Mechanism	Optimization Percentage (%)
Residual torque (N·m)	0.015 ± 0.001	0.009 ± 0.001	40.00 ± 2.7
Peak of residual torque (N·m)	0.12 ± 0.007	0.09 ± 0.007	25.00 ± 1.47
Mass of flywheel (kg)	0.58 ± 0.001	0.23 ± 0.001	60.34 ± 0.11
Balancing time(s)	2.35 ± 0.010	1.15 ± 0.010	51.06 ± 0.22

From the test results, it can be seen that compared with the first-generation torque balancing mechanism, the residual torque of the second-generation torque balancing mechanism proposed in this paper is 0.009 N·m, which is reduced by 40%, the peak of residual torque is 0.09 N·m, which is reduced by 25%, the mass of the balancing flywheel is 0.23 kg, which is reduced by 60.34%, and the torque balancing time is 1.15 s, which is reduced by 51.06%. The range of disturbance that the satellite platform can withstand in the space environment is 1~3 N·m, and the residual torque of the second-generation balancing mechanism is much less than the minimum value of the range and can be considered as having no effect on the satellite. At the same time, according to the design specifications, the peak of the residual moment is not greater than 0.1 N·m, the residual moment is not greater than 0.01 N·m, and the output of the second-generation balancing mechanism meets the design requirements. Considering the existence of uncontrollable factors in the test process, there are errors in the output torque t results between the test and simulation analysis, but the balancing effect is basically the same, so we think the test results are basically consistent with the simulation results, which further reflects the rationality and feasibility of the second-generation torque balancing mechanism proposed in this paper.

6. Discussion

Error is inevitable in the test process and reducing it can improve the reliability of the test and better verify the theoretical feasibility. As can be seen from Figure 11 and Table 5, the residual torque of the torque balancing mechanism of the rotary table proposed in this paper is 0.009 N·m, which is close to 0 N·m, but there is still a small difference from the theoretical analysis. The main reasons are as follows: 1. accumulated installation error: from the power source to the balancing flywheel, it needs to pass through many parts for motion transmission, and there are many parts involved, so the installation error of each part will be accumulated and transmitted continuously, causing the final test result to be different from the theoretical analysis; 2. inaccurate design of component rotational inertia: from Equation (17), it can be seen that there is a definite numerical relationship between the residual torque and the rotational inertia of each component, and the accurate design of component rotational inertia can effectively reduce or eliminate the output torque to achieve the balancing effect; 3. inadequate accuracy and stability of motor angular speed control: Equation (17) is converted from differential form to integral form to show that there is a relationship between the balancing torque and the angular speed of each component, and the accurate output of the angular speed can better achieve torque balancing; 4. errors in measurement results introduced by the experimental setup: this experimental setup provides a degree of freedom of axial rotation to the balancing mechanism by means of a thrust bearing, the lack of precision of the thrust bearing is the main shortcoming of this experimental setup, which affects the accuracy of the test results; and 5. error in the mass distribution of the balancing flywheel: the high-speed rotating flywheel is the key component of this torque balancing mechanism; uneven mass distribution of the flywheel will cause oscillations, resulting in the instantaneous peak of the residual moment to be larger than the average value, which will cause errors in the analysis and processing of the test results. Reducing the errors of the whole system is of great importance for the engineering application of this mechanism.

The balancing mechanism proposed in this paper releases the rotational degrees of freedom of the motor stator for camera attitude adjustment, and the rotor drives the balancing flywheel at high speed through the acceleration mechanism to balance the torque of the rotary table. Under ideal conditions, the attitude adjustment of remote sensing cameras in microgravity environments can be achieved with no effect on the attitude of the satellite platform. Based on the results of the test, the future research directions of the balancing mechanism proposed in this paper are as follows: 1. optimize the structure of the components: optimize the structure of each component by using size optimization and topology optimization to improve the lightness of the whole balancing mechanism; 2. improve machining accuracy: improving machining accuracy can better reduce system errors, which is significant for the subsequent work; 3. optimize the control algorithm of the motor: this paper uses a fuzzy algorithm for motor control, which has good robustness to the system response, but the control accuracy and response speed need to be further optimized. The balancing mechanism proposed in this paper can be applied not only to remote sensing camera attitude adjustment but also to a variety of cases, such as aerial cameras, shipboard cameras, synthetic aperture radar, and so on, which has wide applicability and optimization space. It can be reasonably adjusted according to the actual application and has important value in engineering application and scientific exploration.

7. Conclusions

In this paper, the influence of external torque on satellite attitude is analyzed according to the Newton–Euler method. Based on this analysis, a torque balancing mechanism for a remote sensing camera's two-axis rotary table is proposed based on theories related to momentum moment theorem, momentum moment conservation law, and practical engineering needs, and a detailed study of this mechanism is carried out. Firstly, a theoretical analysis was carried out to derive the numerical relationship between the residual torque and the rotational inertia, dimensions, and angular acceleration of each component. Secondly, the structural design and simulation analysis of the balancing mechanism were carried out. From the simulation analysis, it can be seen that the residual torque of the second-generation torque balancing mechanism proposed in this paper is 0.02 N·m, which is reduced by 66.67%, the peak of residual torque is 0.45 N·m, which is reduced by 57.55%, the mass of the balancing flywheel is 0.15 kg, which is reduced by 74.14%, and the torque balancing time is 0.2 s, which is reduced by 42.86%. Finally, this paper processed and designed the prototype of a torque balancing mechanism and conducted a comparison test. From the test results, it can be seen that the residual torque of the second-generation test prototype is 0.009 N·m, which is reduced by 40%, the peak of residual torque is 0.09 N·m, which is reduced by 25%, the mass of the balancing flywheel is 0.23 kg, which is reduced by 60.34%, and the torque balancing time is 1.15 s, which is reduced by 51.06%. In terms of torque balance, due to the existence of uncontrollable factors in the test, such as assembly accuracy, friction torque, machining errors, etc., there are some differences between the test results and the simulation results, but the overall trend of torque balance is more consistent with the theoretical results and simulation results. In summary, the proposed torque balancing mechanism for a remote sensing camera's two-axis rotary table is feasible and reasonable.

Author Contributions: Conceptualization, Y.W. and C.C.; methodology, Y.W.; software, Y.W., X.S. and T.Z.; validation, Y.W. and X.S.; formal analysis, Y.W.; investigation, Y.W.; resources, Y.W. and C.C.; data curation, Y.W.; writing—original draft preparation, Y.W.; writing—review and editing, Y.W.; visualization, Y.W.; supervision, C.C.; project administration, T.N. and C.C.; funding acquisition, T.N. and C.C. All authors have read and agreed to the published version of the manuscript.

Funding: This research was funded by the National Natural Science Foundation of China, grant number 62105328.

Data Availability Statement: Not applicable.

Acknowledgments: The authors would like to acknowledge the contribution of all authors of this paper and the funding from the National Natural Science Foundation of China. Moreover, the authors thank the editors and reviewers for their time and effort in reviewing this paper.

Conflicts of Interest: The authors declare no conflict of interest.

References

1. Yao, L.; Liu, Y.; He, Y. A novel ship-tracking method for GF-4 satellite sequential images. *Sensors* **2018**, *18*, 2007. [CrossRef] [PubMed]
2. Kopacz, J.R.; Herschitz, R.; Roney, J. Small satellites an overview and assessment. *Acta Astronaut.* **2020**, *170*, 93–105. [CrossRef]
3. Toth, C.; Jóźków, G. Remote sensing platforms and sensors: A survey. *ISPRS J. Photogramm. Remote Sens.* **2016**, *115*, 22–36. [CrossRef]
4. Li, S.; Wang, Y.; Zhang, H.; Yu, F. Thermal analysis and validation of GF-4 remote sensing camera. *J. Therm. Sci.* **2020**, *29*, 992–1000. [CrossRef]
5. Masterson, R.A.; Miller, D.W.; Grogan, R.L. Development and validation of reaction wheel interference models: Empirical model. *J. Sound Vib.* **2002**, *249*, 575–598. [CrossRef]
6. Anthony, T.; Andersen, G. On-orbit modal identification of the Hubble space telescope. In Proceedings of the 1995 American Control Conference-ACC'95, Seattle, WA, USA, 21–23 June 1995; IEEE: Piscataway, NJ, USA, 1995; Volume 1, pp. 402–406.
7. Marble, S.; Tow, D. Bearing health monitoring and life extension in satellite momentum/reaction wheels. In Proceedings of the 2006 IEEE Aerospace Conference, Big Sky, MT, USA, 4–11 March 2006; IEEE: Piscataway, NJ, USA, 2006; p. 7.
8. Kim, D.K. Micro-vibration model and parameter estimation method of a reaction wheel assembly. *J. Sound Vib.* **2014**, *333*, 4214–4231. [CrossRef]
9. Kang, L.; Zhang, H. On-orbit identification of flexible spacecraft and periodic interference based on Subspace Algorithm. In Proceedings of the AIAA Guidance, Navigation, and Control Conference and Exhibit, Providence, RI, USA, 16–19 August 2004; p. 5116.
10. Engelbrecht, J.A.A.; Steyn, W.H. In-orbit identification of unmodelled interference torques acting on a spacecraft body. In Proceedings of the 2004 IEEE Africon. 7th Africon Conference in Africa (IEEE Cat. No. 04CH37590), Gaborone, Botswana, 15–17 September 2004; IEEE: Piscataway, NJ, USA, 2004; Volume 1, pp. 3–8.
11. Goodzeit, N.; Phan, M.; Goodzeit, N.; Phan, M. System and periodic interference identification for feedforward-feedback control of flexible spacecraft. In Proceedings of the 35th Aerospace Sciences Meeting and Exhibit, Reno, NV, USA, 6–9 January 1997; p. 682.
12. Wu, Y.H.; Han, F.; Zheng, M.H.; Wang, F.; Hua, B.; Chen, Z.-M.; Cheng, Y.-H. Attitude tracking control for a space moving target with high dynamic performance using hybrid actuator. *Aerosp. Sci. Technol.* **2018**, *78*, 102–117. [CrossRef]
13. Yao, J.; Hu, Q.; Zheng, J.; Paolo Incremona, G.; Yuca Huanca CP, E.; Colaneri, P. Spacecraft Attitude Reorientation with Reaction Wheel Assembly via State-Dependent Coefficient Parameterizations. *J. Guid. Control. Dyn.* **2022**, *45*, 2147–2154. [CrossRef]
14. King, J.T. Increasing agility in orthogonal reaction wheel attitude control systems. *Acta Astronaut.* **2020**, *177*, 673–683. [CrossRef]
15. Krishna, N.S.; Gosavi, S.; Singh, S.; Saxena, N.; Kailaje, A.; Datla, V.; Shah, P. Design and implementation of a reaction wheel system for CubeSats. In Proceedings of the 2018 IEEE Aerospace Conference, Big Sky, MT, USA, 3–10 March 2018; IEEE: Piscataway, NJ, USA, 2018; pp. 1–7.
16. Nagabhushan, V.; Fitz-Coy, N.G. On-orbit jitter control in momentum actuators using a three-flywheel system. *Acta Astronaut.* **2014**, *95*, 61–81. [CrossRef]
17. Li, L.; Tan, L.; Kong, L.; Wang, D.; Yang, H. The influence of flywheel micro vibration on space camera and vibration suppression. *Mech. Syst. Signal Process.* **2018**, *100*, 360–370. [CrossRef]
18. Jin, J.; Zhang, T.; Kong, L.; Ma, K. In-orbit performance evaluation of a spaceborne high precision fiber optic gyroscope. *Sensors* **2018**, *18*, 106. [CrossRef] [PubMed]
19. Weiyong, Z.; Dongxu, L.I.; Qing, L.; Kun, L. Analysis and testing of microvibrations produced by momentum wheel assemblies. *Chin. J. Aeronaut.* **2012**, *25*, 640–649.
20. Wang, L.H.; Wu, X.Q. Research on neural network control technology for Satellite-based laser communication tracking rotary table. In *Advanced Materials Research*; Trans Tech Publications Ltd.: Stafa-Zurich, Switzerland, 2014; Volume 945, pp. 2266–2271.
21. Gan, K.L.; Ge, S.M.; Wang, L. Application of Compensation Wheel on Satellite. In *Applied Mechanics and Materials*; Trans Tech Publications Ltd.: Stafa-Zurich, Switzerland, 2012; Volume 190, pp. 763–767.
22. Qin, T.; Guo, J.L.; Zhang, M.L.; Han, P.X.; Wang, J.; Qi, B. Structure design and stiffness analysis of spaceborne two-axis rotary table. *Infrared Laser Eng.* **2022**, *51*, 20210364-1–20210364-9.